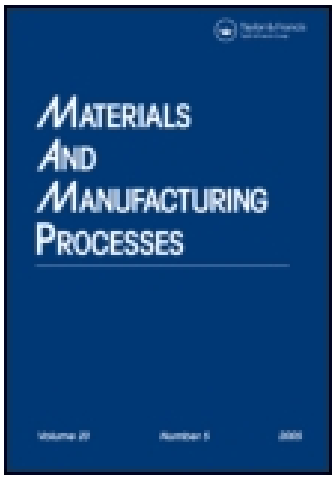

Materials and Manufacturing Processes
Publication details, including instructions for authors and subscription information:
http://www.tandfonline.com/loi/lmmp20

Dissimilar Welding of H62 Brass-316L Stainless Steel Using Continuous-Wave Nd:YAG Laser

Yang Li [a b], Shengsun Hu [a b], Junqi Shen [a b] & Bao Hu [a b]
[a] School of Materials Science and Engineering, Tianjin University, Tianjin, P. R. China
[b] Tianjin Key Laboratory of Advanced Joining Technology, Tianjin University, Tianjin, P. R. China
Accepted author version posted online: 12 Feb 2014.Published online: 18 Jul 2014.

To cite this article: Yang Li, Shengsun Hu, Junqi Shen & Bao Hu (2014) Dissimilar Welding of H62 Brass-316L Stainless Steel Using Continuous-Wave Nd:YAG Laser, Materials and Manufacturing Processes, 29:8, 916-921, DOI: 10.1080/10426914.2013.822981

To link to this article: http://dx.doi.org/10.1080/10426914.2013.822981

Materials and Manufacturing Processes, 29: 916–921, 2014

ISSN: 1042-6914 print/1532-2475 online
DOI: 10.1080/10426914.2013.822981

Taylor & Francis
Taylor & Francis Group

Dissimilar Welding of H62 Brass-316L Stainless Steel Using Continuous-Wave Nd:YAG Laser

Yang Li[1,2], Shengsun Hu[1,2], Junqi Shen[1,2], and Bao Hu[1,2]

[1]*School of Materials Science and Engineering, Tianjin University, Tianjin, P. R. China*
[2]*Tianjin Key Laboratory of Advanced Joining Technology, Tianjin University, Tianjin, P. R. China*

Continuous-wave Nd:YAG laser welding of H62 brass and 316L stainless steel was studied using welded joints made with different overlap configurations. Optical and scanning electron microscopies, energy-dispersive X-ray spectroscopy, and microhardness testing were used to analyze the microstructures and mechanical properties of the joints. The welded joints with the brass-on-steel overlap configuration exhibited better performance. Elemental diffusion and dissolution—in particular, the evaporation of zinc—were observed in the welded joints. Intermetallic compounds were absent in the joints because brass and stainless steel exhibit unlimited solid solubility. Finally, the microhardness of the joints was higher than that of the brass.

Keywords Brass; Dissimilar; Lasers; Microstructure; Stainless; Steel; Welding.

Introduction

In recent years, the joining of dissimilar materials has gained increasing importance, in particular for the purpose of reducing weight and for tailoring component properties. Joints of dissimilar materials are used in complex industrial structures [1–5] to confer both structural and economic advantages. Composite structures of steel and copper alloys are widely employed in the aerospace, machinery, chemical, metallurgical, and refrigeration industries. The joining of steel and copper alloys affords reasonable structures, resulting in savings of large quantities of nonferrous metals. Welding is one of main processing techniques employed for connecting various metallic structural parts.

The differences in the physical properties, including the melting points, coefficients of heat conductivity, and coefficients of linear expansion, as well the mechanical properties, of copper alloys and steel usually result in stress concentration and, consequently, weld cracking in welded joints of these materials. To solve this problem, it is essential to choose an appropriate welding process and structure [6]. Only a few welding methods can be applied to steel and copper or steel and copper alloy welds because of the limitation of space and the differences in their physical and mechanical properties [7].

Traditionally, the processes for forming welds of steel and copper alloys have included ultrasonic welding, friction stir welding, and resistance welding. However, these traditional techniques are restricted in their applicability by the heat that can be input, as well as by their repeatability and flexibility. In contrast to conventional thermal joining processes, heating using a laser beam with a high power density could minimize some of these problems and also allow for effective control of the shape and dimensions of the molten region [8, 9]. The high power density should also cause the welded materials to immediately reach their fusion point despite the difference in their melting temperatures.

Recently, Magnabosco et al. [10] investigated the fusion zone microstructures formed during the electron beam welding of copper plates and plates of three different types of austenitic stainless steels. The results showed the formation of complex, heterogeneous fusion zone microstructures that were characterized by both rapid cooling and poor mixing of the materials. However, the effect of the welding configuration on welded joints is yet to be reported.

Mai and Spowage [11] studied the laser welding of copper and tool steel using a 350 W pulsed Nd:YAG laser. Butt joints produced by the laser beam 0.2 mm off center to the steel did not undergo hot cracking in the heat-affected zone (HAZ). However, the study only researched the melting quantity of copper.

Finally, most previous studies on welding have focused mainly on joints between copper and other metals, and there has been little research on the welding of brass, a copper alloy. Hence, studies on the welding of brass and stainless steel and on the structures and properties of the joints of these materials are required.

Experimental procedure

Materials

The laser welding experiments were performed by forming joints between the two metallic materials (316L

Received April 25, 2013; Accepted June 27, 2013

Address correspondence to Junqi Shen, Room C0804, Building 25, School of Materials Science and Engineering, Tianjin University, Weijin Road 92, Nankai District, Tianjin 300072, P. R. China; E-mail: shenjunqi@tju.edu.cn; liyanghegongda@126.com

Color versions of one or more of the figures in the article can be found online at www.tandfonline.com/lmmp.

TABLE 1.—Chemical compositions (wt.%) of the materials used.

	Cu	Zn	Fe	C	Cr	Ni	Mo	Mn	Si	P
Steel	—	—	69.74	0.026	16.60	10.03	2.06	1.07	0.36	0.027
Brass	64.08	30.57	—	5.35	—	—	—	—	—	—

stainless steel and H62 brass) using two different overlap configurations (brass-on-steel and steel-on-brass). H62 brass is a copper–zinc alloy containing ~62 wt.% copper and ~38 wt.% zinc. Zinc improves the strength and hardness of materials. The austenitic stainless steel 316L possesses high corrosion resistance, owing to the presence of molybdenum. The steel and brass samples used in the study were in the form of sheets 200 mm in length, 50 mm in width, and 0.4 mm in thickness. The chemical compositions of 316L stainless steel and H62 brass are listed in Table 1.

At high temperature, the atomic radii, lattice type, and lattice constant of brass are close to those of steel. Thus, the two materials can form an unlimited solid solution in the liquid phase and a limited solid solution in the solid phase; the formation of intermetallic compounds of these materials is, thus, difficult. The physical properties of brass and steel, including their fusion temperatures, thermal conductivities, and coefficients of linear expansion, are strikingly different. When dissimilar materials like brass and steel are welded, the differences in their physical properties (such as their melting temperatures, coefficients of linear expansion, thermal conductivities, and electrical resistivities, to name a few) generally increase the difficulty of welding. The most important thermophysical properties of the two materials are shown in Table 2.

Experimental Design and Processing Parameters

Before being welded, the brass and stainless steel sheets were polished using 800 grit SiC paper to remove the oxide film from their surfaces. A continuous-wave Nd:YAG laser system (JK2003SM), with a maximum average output power of 2000 W, was used in this study. The focal length and the diameter of the laser beam were 160 and 0.6 mm, respectively. Pure argon (injected at 15 L min^{-1}) was used as the protective gas in all the experiments. As mentioned earlier, two different overlap configurations (S1 and S2) were used and are shown in Fig. 1. S1 is the brass-on-steel configuration, and S2 is the steel-on-brass configuration. The distances from point A to point B and point C to point D were both 25 mm. In addition, the distances from point B to point O and point C to point O were both 12.5 mm. The parameters for the laser welding process are listed in Table 3.

TABLE 2.—Important thermophysical properties of steel and brass at room temperature [12].

Metal	Melting point (°C)	Resistivity (Ω mm^2 m^{-1})	Density (g cm^{-3})	Conductivity (W $(m°C)^{-1}$)	Heat capacity (J kg^{-1} K^{-1})	Coefficient of linear expansion
Steel	1371	0.71	7.98	14 ~ 21	485	16.0
Brass	934	0.071	8.5	108.9	390	20.6

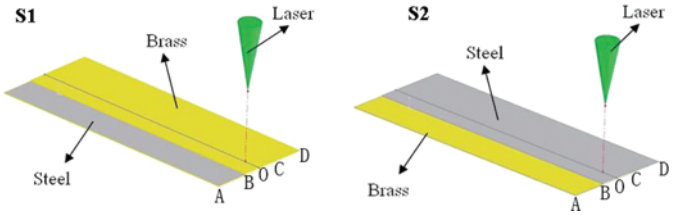

FIGURE 1.—The overlap configurations used to form the welded joints.

TABLE 3.—Process parameters used to form the welded joints.

Overlap configuration	Power (W)	Welding speed (mm s^{-1})
S1	1370	40
S2	1315	40

The surfaces of the welded samples were polished and etched after the completion of the laser welding process. Two etchants were used to reveal the microstructures of the cross sections of the welded samples. First, the brass side of the welded samples was etched with a solution consisting of 59 g of $FeCl_3$, 20 mL of HCl, and 96 mL of C_2H_5OH. Then, the microstructure of the etched brass was observed using optical microscopy. After the etching of the brass side, the stainless steel side was etched with a mixture of 30 mL of HCl, 10 mL of HNO_3, and 10 mL of $C_3H_8O_3$ (glycerol). Subsequently, the microstructure of the etched stainless steel was observed using optical microscopy. The microstructure of the interface and its elemental composition were determined using scanning electron microscopy (SEM) and energy-dispersive X-ray spectroscopy (EDS), respectively. The microhardness (determined using a load of 1000 g) of the joints was measured using a Vickers microindentation tester.

RESULTS AND DISCUSSION

Microstructures of the Welded Joints

The microstructures of brass in the welded joints S1 and S2 are shown in Figs. 2 and 3, respectively. Figure 2(a) shows that the welded-metal zone in the S1 joint had a minimum grain-dendritic structure. Figure 2(b) shows the microstructure of the fusion zone, which is characterized by lamellar and acicular structures with Widmanstätten features. Figure 2(c) shows that the HAZ also contained the lamellar and acicular structures, albeit with a finer microstructure than that in the fusion zone. During the welding process, the phase α began to separate along the habit planes of the phase β owing to the high cooling rate and high zinc content. The distance between the HAZ and the welded metal was greater than that between the fusion zone and the welded metal. Therefore, the grains of the HAZ were finer than those of the fusion zone. Further, the

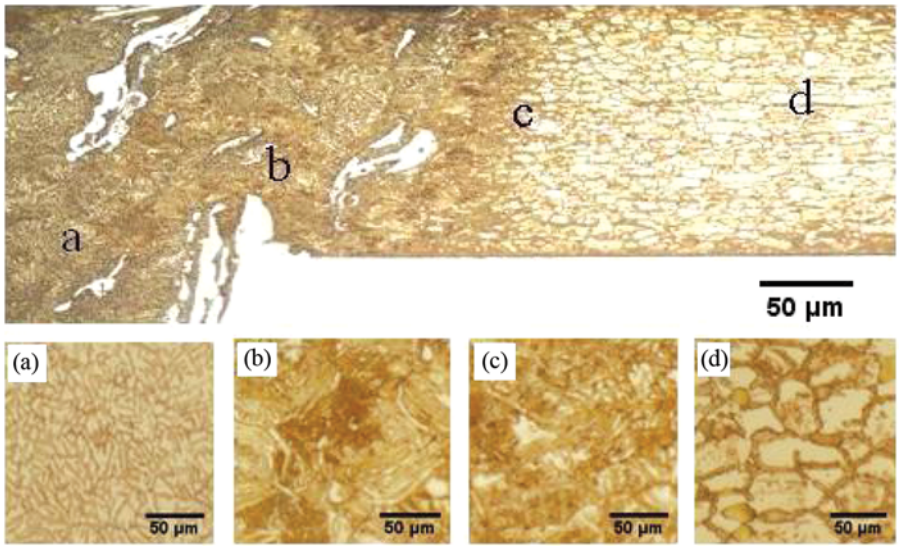

FIGURE 2.—Microstructure of brass in the welded zone of the S1 joint: (a) Welded-metal zone. (b) Fusion zone. (c) Heat-affected zone. (d) Base metal.

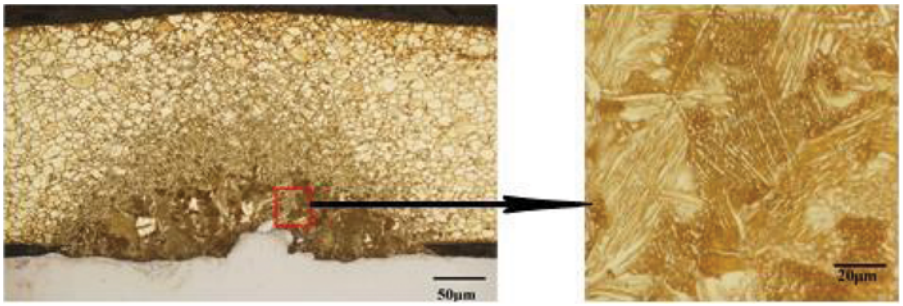

FIGURE 3.—Microstructure of brass in the welded zone of the S2 joint.

microstructure of the base metal consisted of cold-rolled grains. Of the four zones (a, b, c, and d) of the welded joint, the grains of the fusion zone were the most coarsened; it is likely that this contributes to the brittleness of the welded S1 joint.

Figure 3 shows that the welded-metal zone of the S2 joint consisted of the most coarsened crystals with lamellar and acicular structures in the four zones of the entire welded joint. These coarsened grains resulted in fracture and failure. Hence, because of its poor mechanical performance, the configuration S2 was found to be unsuitable for industrial applications.

Figure 4 shows the microstructures of stainless steel in the welded zones of the S1 and S2 joints. In the S1 configuration, steel exhibited an isometric austenite microstructure, and in S2, it showed perfect recrystallization.

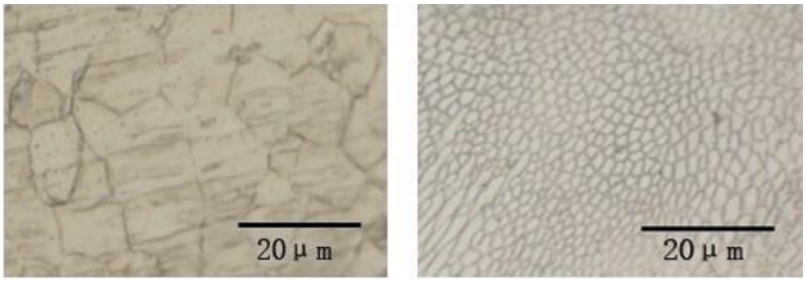

FIGURE 4.—Microstructures of stainless steel in the welded zones of the S1 and S2 joints.

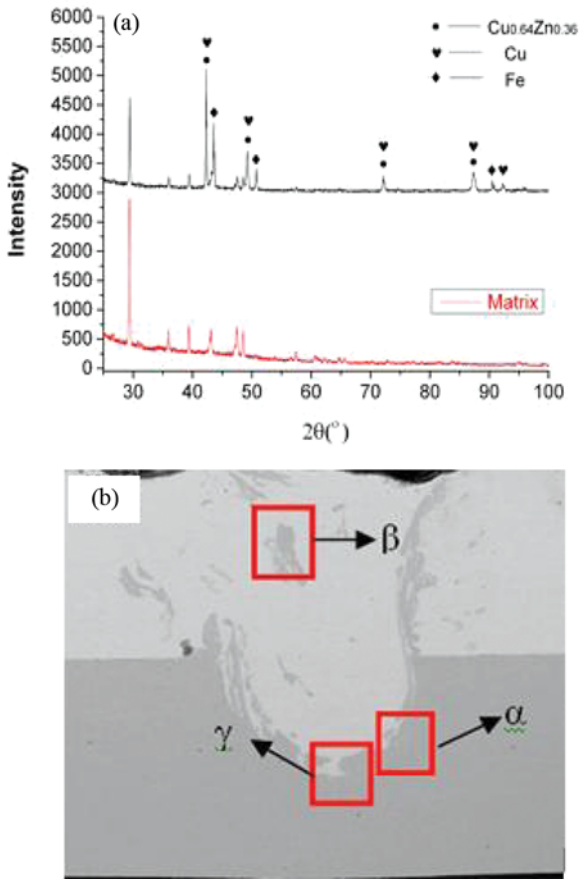

FIGURE 5.—XRD results of the welded joint and microstructure.

The microstructure of the welded joint with the S2 configuration resulted in poor mechanical properties. This is another reason the overlap configuration S1 is more suitable for the laser welding of H62 brass and 316L stainless steel, as shown in Figs. 2 and 3. The most likely reason is the presence of zinc, which has low melting and boiling points, in brass. As a result, it was easier to achieve laser penetration during welding using the configuration S1.

Chemical Compositions of the Welded Joints

The configuration S1 resulted in a more homogeneous mix. In addition, it was found that in the configuration S1, there is no intermetallic compound in the welded joint. The phase in the welded joint was identified as the Cu0.64Zn0.36, Cu, and Fe phase by X-ray diffraction (XRD), as shown in Fig. 5(a). Meanwhile, some of the steel penetrated into the brass (see the area β of Fig. 5(b) and Point B of Fig. 6. However, brass penetration into steel was not noticed in the configuration S2, meanwhile, the EDS results (listed in Table 4) showed that Point B was rich in Fe and relatively poorer in copper and zinc; this was further proof of the penetration of steel into brass, which took place because brass and steel can form an unlimited solid solution in the liquid phase and because the density of stainless steel is less than that of brass. This was reason that differences were noticed in the microstructures of the joints formed using the configurations S1 and S2.

Since the overlap configuration S2 was found to unsuitable for the laser welding of H62 brass and 316L stainless steel, this configuration is not discussed further.

Figure 6(a)–(d) displays magnified images of the three zones enclosed in red squares in Fig. 5(b). Point A in Fig. 6(a) indicates a microcrack in the area α in Fig. 5(b). Point B in Fig. 6(b) indicates the dark globules seen in the area β in Fig. 5(b). Point C in Fig. 6(c) is the stainless steel side of the area γ in Fig. 5(b). Finally, Point D in Fig. 6(d) is the brass side of the area γ in Fig. 5(b).

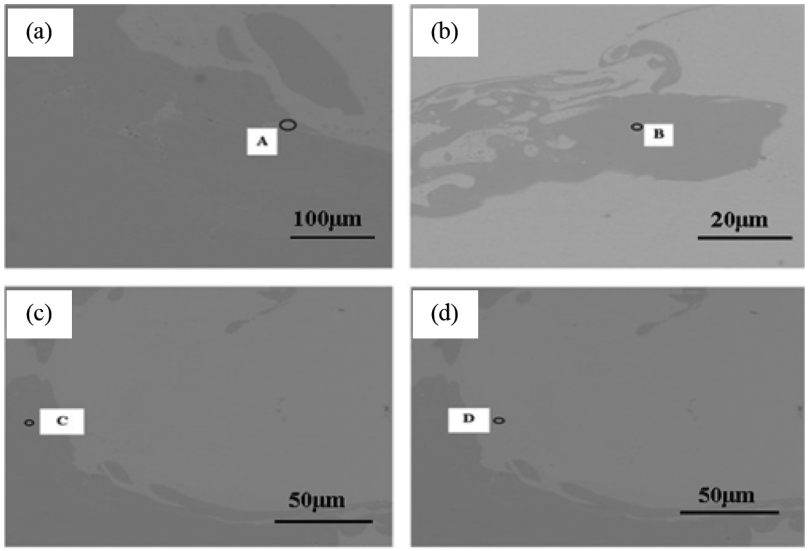

FIGURE 6.—High-magnification SEM micrographs of the welded joint shown in Fig. 5.

TABLE 4.—Chemical compositions (in wt.%) of points A, B, C, and D.

	Fe	Cr	Ni	C	Si	Mn	Mo	Cu	Zn
Point A	19.85	5.38	3.36	6.58	—	—	—	42.58	19.21
Point B	63.80	15.95	9.42	—	0.51	1.62	2.34	6.36	—
Point C	60.13	15.35	8.96	—	0.63	1.50	2.11	11.32	—
Point D	—	—	—	—	—	—	—	62.81	31.79

Table 4 shows the results of the EDS analyses performed on Points A, B, C, and D in Fig. 6. It can be seen from Table 4 that Point A of the microcrack in the area α was composed only of copper and zinc, indicating that copper and zinc penetrated into the steel and formed microfissures. This is because the thermal conductivity of brass is much higher than that of stainless steel, as shown in Table 2.

It can also be seen from Table 4 that Point C contained higher amounts of copper and zinc than did Point B, indicating that the degree of mixing of the metallic materials (brass and stainless steel) in the welded joint was higher than that in the other areas. Finally, Point D was rich in copper and zinc and did not contain any Fe and Cr.

It can be seen from Fig. 6 and Table 4 that intermetallic phases were absent in the interface and that only two phases, one rich in copper and zinc and the other rich in steel, were present in the microstructures of the welded joints. This could be caused by a number of reasons, including the low solubility between steel and brass in the solid state and the high heating and cooling rates associated with laser welding.

Figure 7 shows that there was some variation in the amounts of Cr, Fe, and Ni found in the welded S1 joint. This was further proof that a small amount of steel penetrated into the brass. It should be noted that zinc does not evaporate readily.

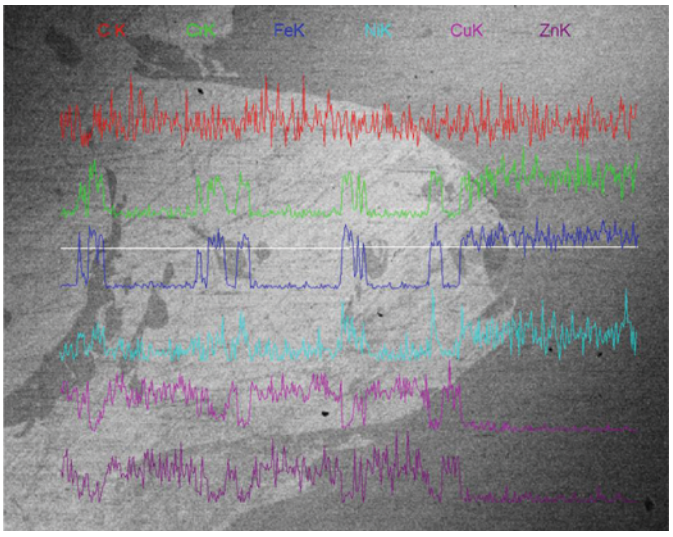

FIGURE 7.—Line profiles across the interface of the welded joint made using the configuration S1.

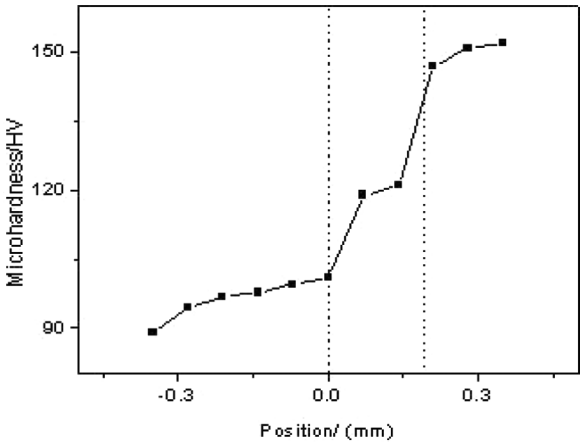

FIGURE 8.—Distribution of the microhardness across a welded joint.

Hardness of the Joint Made Using the Configuration S1

Figure 8 shows the results of the microhardness test performed on the H62 brass-316L stainless steel joint made using the configuration S1. The microhardness of the welded joint was higher than that of brass and lower than that of stainless steel. This may be attributed to the rapid heating and cooling that takes place during the laser welding process; this resulted in grain refinement, which caused the hardness of the welded joint to become higher than that of brass. Thus, the desired result that the hardness of the welded joint should be higher than that of the base metals was achieved.

CONCLUSIONS

1. Because of the difference in the densities of brass and stainless steel and owing to the fact that the melting temperature of Zn present in brass is lower, welded joints of H62 brass H62 and 316L stainless steel having a sound microstructure and interface could be obtained with the S1, i.e., the brass-on-steel, overlap configuration.
2. The microstructure of the welded joints could be divided into four zones. The metallographic structure of brass showed that the fusion zone had a lamellar structure and contained the most coarsened grains; it is likely that this causes the brittleness of the welded joints.
3. Intermetallic compounds were absent at the interface, and a mixture of two nonequilibrium phases, one rich in Cu and Zn and the other rich in Fe, Cr, and Ni, was observed. The evaporation of Zn in the welding line was not noticed.
4. The microhardness of the welded joints was higher than that of the brass; this was because the grains of the joints underwent refinement during the welding process. The microhardness of the welded joint zone containing the refined grains was greater than that of the brass by about 30 HV.

Funding

The authors gratefully acknowledge support from the National Natural Science Foundation of China (Grant No. 50975195).

References

1. Sierra, G.; Wattrisse, B.; Bordreuil, C. Structural analysis of steel to aluminum welded overlap joint by digital image correlation. *Experimental Mechanics* **2008**, *48*, 213–223.
2. Torkamany, M.J.; Tahamtan, S.; Sabbaghzadeh, J. Dissimilar welding of carbon steel to 5754 aluminum alloy by Nd:YAG pulsed laser. *Materials and Design* **2010**, *31*, 458–465.
3. Sun, Z. Fusion zone microstructures of laser and plasma welded dissimilar steel joints. *Materials and Manufacturing Process* **1999**, *14* (I), 37–52.
4. Kandasamy, J.; Manzoor Hussain, M.; Rajesham, S. Heterogeneous friction stir welding: Improved properties in dissimilar aluminum alloy joints through insertion of copper coupled with external heating. *Materials and Manufacturing Processes* **2012**, *27*, 1429–1436.
5. Esmaeili, A.; Besharati Givi, M.K.; Zareie Rajani, H.R. Experimental investigation of material flow and welding defects in friction stir welding of aluminum to brass. *Materials and Manufacturing Processes* **2012**, *27*, 1402–1408.
6. Yao, C.; Yao, B.; Zhang, X.; Huang, J.; Fu, J.; Wu, Y. Interface microstructure and mechanical properties of laser welding copper-steel dissimilar joint. *Optics and Lasers in Engineering* **2009**, *47*, 807–814.
7. Luo, J.; Wang, X.; Liu, D.; Li, F.; XiangInertia, J. Radial friction welding joint of large size H90 brass/D60 steel dissimilar metals. *Materials and Manufacturing Processes* **2012**, *27*, 930–935.
8. D'Amato, C.; Fenech, M.; Abela, S.; Betts, J.C.; Buhagiar, J. Autogenous laser keyhole welding of AISI 316LTi. *Materials and Manufacturing Processes* **2010**, *25*, 1269–1277.
9. Chen, Q.; Yan, H.; Chen, J.; Zeng, P.; Yu, Z.; Su, B. Laser beam welding of AZ31 magnesium alloy with filler strip. *Materials and Manufacturing Processes* **2010**, *25*, 1227–1232.
10. Magnabosco, I.; Ferro, P.; Bonillo, F.; Arnberg, L. An investigation of fusion zone microstructures in electron beam welding of copper- stainless steel. *Materials Science and Engineering A* **2006**, *424* (1), 63–173.
11. Mai, T.A.; Spowage, A.C. Characterisation of dissimilar joints in laser welding of steel-kovar, copper-steel and copper-aluminum. *Material Science and Engineering A* **2004**, *374*, 224–233.
12. Smittells, C.M. *Metals Reference Book*, 5th ed.; Butterworth: London, 1976.